Segmentation using vector-attribute filters: methodology and application to dermatological imaging

Benoît Naegel[1,2], Nicolas Passat[3], Nicolas Boch[4] and Michel Kocher[1]

[1] *EIG-HES, Geneva School of Engineering, Geneva, Switzerland*
`{benoit.naegel,michel.kocher}@hesge.ch`

[2] *LORIA, Campus Scientifique, Vandœuvre-les-Nancy, France*

[3] *LSIIT, UMR 7005 CNRS/ULP, Strasbourg 1 University, France*
`passat@dpt-info.u-strasbg.fr`

[4] *Digital Imaging Unit, Department of Radiology, Geneva University Hospital, Switzerland*

Abstract   Attribute-based filters can be involved in analysis and processing of images by considering attributes of various kinds (quantitative, qualitative, structural). Despite their potential usefulness, they are quite infrequently considered in the development of real applications. A cause of this underuse is probably the difficulty to determine correct parameters for non-scalar attributes in a fast and efficient fashion. This paper proposes a general definition of vector-attribute filters for grey-level images and describes some solutions to perform detection tasks using vector-attributes and parameters determined from a learning set. Based on these elements, an interactive segmentation method for dermatological application has been developed.

Keywords: vector-attribute filters, component-tree, segmentation, dermatological imaging.

1.   Introduction

Connected operators are fundamental tools of mathematical morphology: area filters [20, 21], contrast filters [5], or volumic filters [19] are all connected operators that, given some criteria, simplify the partition of an image without introducing new contours. Attribute openings and thinnings have been introduced in [1] and generalise the notion of connected filters based on arbitrary attributes.

These filters can be efficiently implemented using a tree structure known in the literature as *dendrone* [2,6], *component-tree* [10], *confinement tree* [8] or *max-tree* [13]. In the sequel we will employ the generic term *component-tree* to denote all these tree-like structures. Their main principle consists

in storing each connected component of the successive threshold sets of a grey-level image in a node, and to code the inclusion relation on components by establishing links between the corresponding nodes. To each node of the tree can be associated a real-valued attribute, leading to an efficient tool to design connected, anti-extensive filters [13]. Recently, multi-valued attributes have been considered leading to vector-attribute filters [16].

Such filters seem to have an interesting potential for real application development. However, their main drawback is that attribute parameters are still mainly determined in an empirical fashion, as in [7] where the classification between an object component and the background is made by observation of the attribute signature of this component.

Until now, attribute-filters have been essentially used for removing components presenting undesirable attributes. We wish to demonstrate here that attribute-filters, and more especially vector-attribute filters, can also be efficiently involved in the design of segmentation methods.

This paper is organised as follows. Section 2 presents recent works related to the development of attribute-based filters and their use for applicative purpose. In Section 3 we propose a definition of vector-attribute filters for grey-level images and propose to use them in an object-detection context. Section 4 describes an applicative study of the proposed methodology devoted to the interactive analysis and segmentation of melanocytic nevi in 2D dermatological images. In Section 5 possible developments, improvements and further works are discussed.

2.   Related work

Attribute-based filtering using component-trees has been used in various contexts, including feature extraction and retrieval [2], image coding and compression [13], or segmentation of vessels in wood micrographs [7]. Component-trees have also been used in the field of cerebral segmentation, for the automatic selection of markers from 3D MRI images [3].

The notion of shape-based attributes has been considered in [16–18] as well as the notion of shape granulometry. These concepts have been applied to filament extraction in MR angiograms [18] and classification of diatoms [17].

Component-tree representation of an image based on a connectivity map (leading to a second-order connectivity) has been proposed in [11, 12] and applied to 3D filament extraction in MR angiograms and extraction of filamentous structures in images of proteins.

Vector-attribute filters have been introduced recently in [16], where their use was illustrated on synthetic images of characters, in the context of object filtering based on Hu's moments invariants. Although vector-attribute based filters seem to have a great potential, they have not been used until now in concrete applications.
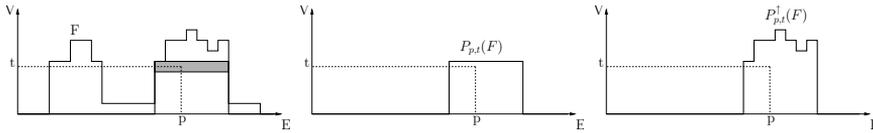
Figure 1. Decomposition of a function into its peak components. Left: Original function F. In grey: connected component of $X_t(F)$ including p. Middle: Peak component $P_{p,t}(F)$. Right: Lobe component $P^{\uparrow}_{p,t}(F)$.

3.   Grey-level vector-attribute filters

The connected components of all threshold sets of an image are usually called *peaks*. In the context of object recognition or segmentation, it could be interesting to detect from a grey-level image the peaks representing a specific structure: only these peaks will be preserved, while all other peaks will be removed.

Formally, a grey-level image is defined as a numerical function $F : E \to V$, where E is a space of points and V a totally ordered set of values, where $\perp$ (resp. $\top$) represents the least (resp. the greatest) element.

The threshold set of a function is defined by $X_t(F) = \{p \in E \mid F(p) \geq t\}$. Given a connectivity class $\mathcal{C}$ on E (i.e., the set of all connected sets), the connected opening for sets is defined as [15]: $\gamma_x(X) = \bigcup \{C \mid x \in C \subseteq X, C \in \mathcal{C}\}$.

We define the peak function $P_{p,t}(F)$ by:

$$P_{p,t}(F)(x) = \left\{ \begin{array}{ll} t & \text{if } x \in \gamma_p(X_t(F)), \\ \perp & \text{otherwise.} \end{array} \right.$$

Any function F is the supremum of all its peak components:

$$F = \bigvee \{P_{p,t}(F) \mid p \in E, t \in V\}.$$

We define the lobe (or superior peak), as:

$$P^{\uparrow}_{p,t}(F)(x) = \left\{ \begin{array}{ll} F(x) & \text{if } x \in \gamma_p(X_t(F)), \\ \perp & \text{otherwise.} \end{array} \right.$$

These functions are illustrated in Figure 1.

Given a valuation function $\tau : V^E \to \mathbb{R}^N$ that associates to a function F a vector of real-valued attributes $\tau(F)$, and a criterion $T : \mathbb{R}^N \to \{true, false\}$ that accepts or rejects an attribute-vector depending on a particular strategy, a grey-level vector-attribute filter ϕ can be defined by acting separately on the peak components of an image:

$$\phi(F) = \bigvee \{P_{p,t}(F) \mid p \in E, t \in V, T(\tau(P^{\uparrow}_{p,t}(F))) = true\}. \qquad (1)$$

The reconstruction of the lobes can be obtained in the same way:

$$\phi^{\uparrow}(F) = \bigvee \{P_{p,t}^{\uparrow}(F) \mid p \in E, t \in V, T(\tau(P_{p,t}^{\uparrow}(F))) = true\}. \qquad (2)$$

In the case where all peak functions are removed, the result of these filtering operations is the least element of the complete lattice of functions V^E: $\bigvee \emptyset = C_{\perp}$ (where $C_{\perp}$ is the constant function defined by: $\forall p \in E, C_{\perp}(p) = \perp$). These filters associate to each lobes of a function a vector of attributes. Using lobes allows to consider non-flat attributes like contrast (i.e., height), or volume of the peak component. If one of the vector-attribute component is non-flat, ϕ is no longer idempotent since it reconstructs only the peak $P_{p,t}$[1]. On the contrary, $\phi^{\uparrow}$ is idempotent, since the lobes verifying the criterion are preserved. These filters are not increasing most of the time, since the criterion based on a vector-attribute is seldom increasing. Hence, they are not *morphological* filters. They are anti-extensive, as they remove peaks from the original function. Finally, as they act only by merging image flat-zones, they are connected operators.

3.1 Object detection

The filters previously described can be used to perform object detection from a grey-level image provided that objects of interest correspond to some peaks of the image: this requires the object to be a bright structure surrounded by dark background (at least after some kind of preprocessing). Such a strategy requires one to have some prior knowledge about the object to segment.

A typical example of criterion (also proposed in [16]) is based on a distance d from a reference vector $\mathbf{r}$:

$$T_{\mathbf{r},\varepsilon}(\mathbf{v}) = \begin{cases} true & \text{if } d(\mathbf{r},\mathbf{v}) < \varepsilon, \\ false & \text{otherwise.} \end{cases}$$

In this latter case, note the difference with the vector-attribute defined in [16]: here peaks are suppressed when their attribute-vectors have a distance superior to ε. In [16], the opposite was performed in order to remove sets having attributes close to the reference vector.

3.2 Vector-attribute filtering using component-tree

Vector-attribute filters, as defined previously, can be efficiently implemented using the image component-tree. Moreover, as we will see in the sequel, the component-tree only needs to be computed once, allowing one to perform multiple consecutive filtering with different parameters $\mathbf{r}$ and ε. The

---

[1]For the same reason, h-reconstruction or volumic filters are not idempotent and hence are not morphological filters.

component-tree of a function F can be defined as follows. Each node of the tree is a peak function belonging to the set: $P(F) = \{P_{p,t}(F) \mid p \in E, t \in V\}$. For $G : E \to V$, we consider the function:

$$supp(G) = \left\{ \begin{array}{ll} \{p \in E \mid G(p) > \bot\} & \text{if } G \neq C_{\bot}, \\ E & \text{if } G = C_{\bot}. \end{array} \right.$$

A node P_2 is a child of P_1 in the component-tree of F ($P_1, P_2 \in P(F)$) iff:

(i) $supp(P_2) \subset supp(P_1)$,

(ii) $\forall P_3 \in P(F), supp(P_2) \subset supp(P_3) \Rightarrow supp(P_1) \subseteq supp(P_3)$.

The root of the component-tree of F is the node $R \in P(F)$ such that $supp(R) = \bigcup_{P \in P(F)}\{supp(P)\} = E$. In particular, $R = C_{F_{min}}$, where $F_{min} = \min\{F(p) \mid p \in E\}$.

Algorithmically, each node can be modelled as a structure : $node = (label, gl,$
$size, att, points, parent, children, active)$, where:

- $label$ is the identifier of the node;

- gl is the grey-level of the node ($gl(P) = \max\{F(p) \mid p \in supp(P)\}$);

- $size$ is the size of the node ($size(P) = card(supp(P))$);

- att is a list of attributes, representing the attribute-vector attached to the node;

- $points$ is the list of points belonging to the node;

- $parent$ is a pointer to the parent;

- $children$ is a list of pointers to the node's children;

- $active$ is a Boolean value indicating the status of the node.

It is desirable to exploit the redundancy of the points belonging to the support of the peaks: each point p can be stored in only one node ($P_{p,F(p)}(F)$). This is the principle adopted in [13], leading to the max-tree. In this case, some nodes have no points: they can be suppressed, leading to the unique representation of the tree [8]. The construction of the component-tree can be done using efficient algorithms [8, 10, 13].

Given a valuation function τ and a criterion T, an image filtered by applying Equation 1 can be processed by computing the component-tree of the original image and reconstruct only the nodes verifying T: this is equivalent to prune the tree using the *direct* decision [13], as illustrated in Figure 2. A tree-based filtering can be decomposed into three steps: component-tree computation; tree filtering; image restitution using the *direct* strategy.
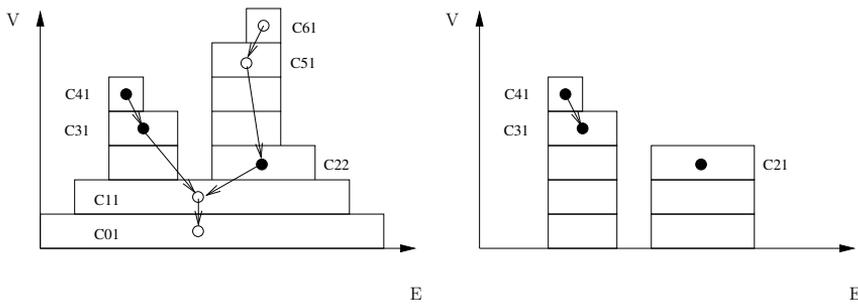
Figure 2. Left: Original image. Empty circles denote nodes that do not meet a considered criterion. Right: Direct reconstruction of peak functions that meet this criterion (applying equation 1).

3.3 Attributes

To each lobe of a function is attached a vector of attributes generated by the τ function. Vector-attributes can represent any combination of photometric, textural, or geometric attributes. The attributes most usually considered for the design of component-tree methods are intensity, area, height (or contrast), and volume, the last two one being defined by:

- Height (or contrast): $height(P^\uparrow) = \max_{p \in supp(P^\uparrow)}\{F(p) - gl(P^\uparrow) + 1\}$,

- Volume: $volume(P^\uparrow) = \sum_{p \in supp(P^\uparrow)}\{F(p) - gl(P^\uparrow) + 1\}$.

Geometric or shape attributes have an interesting potential since they enable to discriminate an object by considering its structural properties, by opposition to more classical photometric properties. In [22], various shape representation techniques are described, which could lead to the computation of such attributes. However when using the component-tree, it is desirable (for efficiency reasons) to use attributes that can be computed incrementally during its construction.

3.4 Attribute learning from a reference component-tree

Using vector-attribute filters for object detection requires a preliminary characterisation of a specific class of objects. A possible way to retrieve some information regarding the attributes of a class is to use a set of object samples (or learning set). This learning set can be composed, for example, of manually delineated structures on some original images. Given images F_i in which the structures of interest have been segmented (each structure being a connected set S_i), it is possible to extract, for each manually segmented component, the most corresponding peak of F_i. This can be done

using the component-tree of F_i: to each point of the manual segmentation $p \in S_i$ is associated the corresponding node or peak function $P_{p,F(p)}(F)$. Algorithmically, this correspondence can be carried out using a mapping between the points and their corresponding nodes. To each component S_i is associated a set of potential peaks. A way to process this can consist in retrieving the node associated to the peak having the closest size to the component's size (i.e., $card(S_i)$).

The attribute-vector of the node can then be retrieved and associated to the component S_i. The set of attribute-vectors corresponding to the manually segmented structures represent the learning set of the structure of interest.

4. Application: Segmentation of melanocytic nevi from photographs of the whole body

Early detection of skin cancer is a very important issue to prevent the mortality due to this kind of affection. Computer-aided diagnosis represents one step towards a more accurate and faster detection of suspicious moles. Much of the research effort in this domain has been done in the field of automated diagnosis from dermatoscopy examinations [4,14]. However this kind of methods requires the dermatologist to detect beforehand the suspicious lesions, which is difficult due to the large number of moles in the patients at risk.

Mole mapping from digital photographs is a relatively recent method whose purpose is to assist the dermatologist in the detection of suspicious moles. To this aim, a cartography of the existing moles is performed from images of the whole body acquired at different times. Changes can be tracked by comparing automatically the corresponding moles in the different images.

In previous work, a mole-mapping system has been proposed [9], enabling the detection of the moles in several images of a patient and the matching of the corresponding structures. Although based on empirically evaluated parameters, the method was automatic and efficient due to the component-tree approach. We propose here an improved method which allows the dermatologist to segment interactively a class of moles of interest (for example only the largest ones) and to use the specific parameters of this class to infer the segmentation of the closest moles belonging to the same one.

4.1 Definitions and notations

Photographs of the whole body are considered as functions $F : E \rightarrow \mathcal{T}^{rgb}$ where $\mathcal{T}^{rgb} = \mathcal{T}^r \times \mathcal{T}^g \times \mathcal{T}^b$ represents the set of colour values defined by a triplet (r, g, b). Images are processed in the saturation space to discriminate

moles from skin: indeed, moles and skin have similar hue, but moles appear more saturated than the skin. The saturation image is defined by the function: $S : E \to \mathcal{T}^s : x \mapsto \frac{max-min}{max}$ where max (resp. min) represents the largest (resp. the smallest) value of the RGB triplet $F(x) = (r, g, b)$. We define $S(x) = 0$ for $F(x) = (0, 0, 0)$. An original image, and a sample visualised in the saturation space, are illustrated in Figure 3.

Figure 3. Left: Original image F (visualised in grey-levels, but defined in the RGB colour space). Right: Enlargement of the white-bordered zone, in the saturation image S associated to F.

4.2 Interactive segmentation algorithm

Photographs of the whole body consist in a total of 16 images of a patient in the front, back, right and left positions. The acquisition of each image set requires a calibration of the digital camera. Dimensions of each image are 4288×2848 (12 megapixels). The corresponding physical size of the image pixels obtained from the calibration step is typically contained between 0.16 and 0.17 mm. Individual images of the corresponding part of the body are then selected by the practitioner for the examination.

Input and output   The segmentation algorithm takes as input two digital photographs of similar parts of the body acquired at different times. The practitioner can interactively contour the moles of interest, providing a first manual segmentation. A minimum of three or four segmentations is required to obtain sufficient data for the computation of a statistical model. A distance parameter can be chosen interactively. As output, the algorithm detects the moles which are the closest from the manually selected ones, given the chosen distance parameter. The mole segmentation in each of the image can then be used as the input of a specific point matching algorithm (not described here) [9].

Attributes and criterion In the saturation images, moles appear as bright and compact structures. Cutaneous surfaces have uneven illumination: segmentation methods based on global threshold are not sufficient to discriminate moles from other bright structures (see Figure 3 right, the umbra under the arm appears very bright in the saturation image). To each lobe $P^\uparrow(S)$ of the saturation image can be associated a vector-attribute composed of area, contrast, and compacity parameters:

$$\tau(P^\uparrow(S)) = (area(P^\uparrow(S)), contrast(P^\uparrow(S)), compacity(P^\uparrow(S))).$$

The compacity parameter can be a measure of roundness (for example the ratio $\frac{4\pi A}{P^2}$)), where A and P represent the area and perimeter of the component, respectively. The perimeter can be approximated by using the number of contour points of the component, however this attribute cannot be computed incrementally (it can however easily be computed afterwards using a mapping between the points and the nodes). Hence an alternative is to use the first Hu's invariant moment, that can be computed incrementally as suggested in [17]. The two variants of compacity have been experimentally tested with similar results.

As a criterion, we use $T_{\mathbf{r},\varepsilon}$, in order to suppress peaks that differ of more than a certain quantity ε from a reference vector. The subset of manually segmented moles is used to select, for each connected component, the closest corresponding nodes of the component-tree, using the strategy described in Section 3.4. The set of vector-attributes $\{\mathbf{v_i}\}$ of all selected nodes is used to compute a reference vector:

$$\mathbf{r} = \frac{1}{N}\sum_{i=1}^{N}\mathbf{v_i},$$

and a covariance matrix:

$$\Sigma = \frac{1}{N}\sum_{i=1}^{N}(\mathbf{v_i} - \mathbf{r})^T(\mathbf{v_i} - \mathbf{r}),$$

where N is the number of manually segmented moles.

Segmentation step Assuming that the distribution of the vector-attributes of the moles is Gaussian multivariate, we can consider the statistical model computed previously to use normalised distances. Given the reference vector $\mathbf{r}$ and the covariance matrix Σ, a distance is computed between $\mathbf{r}$ and the vector-attributes $\mathbf{x}$ of all the nodes of the component-tree. This distance expresses the probability that the node belongs to the class selected by the practitioner. This distance can be the Mahalanobis distance:

$$d_M(\mathbf{x}, \mathbf{r}) = \sqrt{(\mathbf{x} - \mathbf{r})^T\Sigma^{-1}(\mathbf{x} - \mathbf{r})}.$$

Hence parameter ε in the criterion $T_{\mathbf{r},\varepsilon}$ defines the sensitivity of the detection. Choosing $\varepsilon = 1.0$ ensures that the selected components are "not farther" than one standard deviation from the reference vector.

4.3   Experiments and results

Experiments have been made on 12 image series. The computation time of the component-tree using Salembier's recursive algorithm[2] is 8 seconds on a Pentium IV 3.2 GHz with 2 Gb of RAM. Each filtering step is made in constant time (0.1 s), allowing an interaction of the dermatologist in real-time.

Some results are illustrated on Figure 4 (for representation purpose, only an enlarged portion of the processed image is shown) for two different sets of manually segmented moles. In the first row the largest moles are detected, while in the second row, only the smallest ones are preserved due to the different training sets. Segmentation is precise since the attribute filter is a connected operator: detected contours correspond to true contours of the detected component. The segmentation method allows a very good discrimination between moles and other bright structures of the saturation image: there is no false detections. This is mainly due to the chosen criteria. Visual assessment of the detected moles by dermatologist tends to prove that the method is very satisfying from a medical point of view. As the chosen attributes are highly uncorrelated in this application, Mahalanobis distance and normalised Euclidean distance give comparable results.

5.   Conclusion and further works

In this paper we have proposed a general definition of vector-attribute filters for grey-level images. This definition allows to filter the function peaks given a vector-attribute and a criterion. We have shown that this definition can be efficiently implemented using the component-tree and the *direct* pruning strategy. Some solutions for using vector-attributes and involving them in the development of component-tree-based filtering processes (especially devoted — but not restricted to — segmentation) have been proposed. They constitute an initial and partial methodological framework which will be enriched in further works.

This framework has been used for the proposal of a segmentation method of dermatological 2D data, allowing a real-time interaction with the practitioner. The efficiency of this method is satisfying from a medical points of view, but also from a theoretical one. Indeed, it tends to prove that it is

---

[2]According to [10], Salembier's algorithm is quadratic in the worst case; however it is generally twice as fast as Najman's one in practical cases when the value of a point is comprised between 0 and 255.

possible to create efficient, fast and easy to use methods for object detection purpose, based on vectorial attribute filters and component-trees.

Further work will now consist in developing this methodology, by integrating more descriptive attributes (for example structural shape descriptors) and extending it to classification tasks.
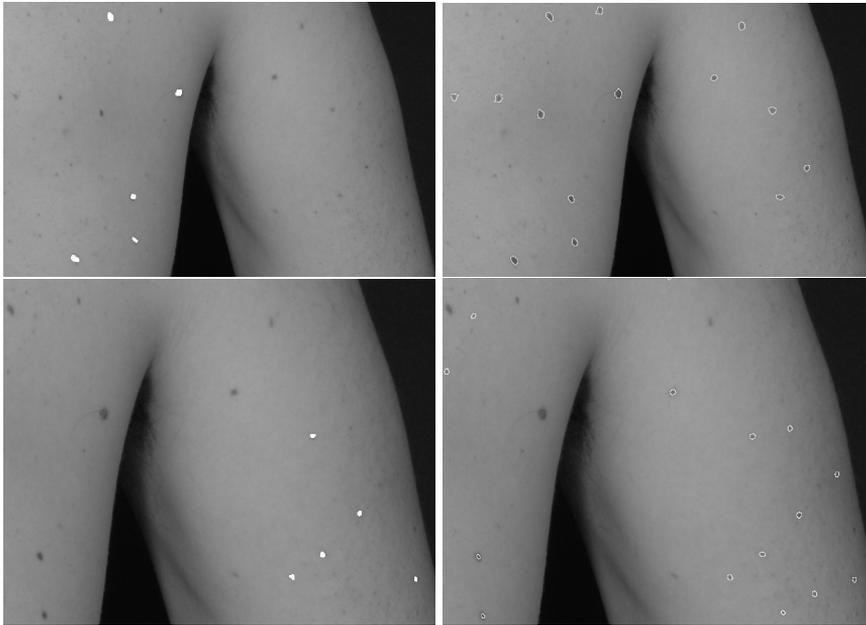
Figure 4. First column: 5 manually segmented moles (in white). Second column: Moles segmented using a normalised Euclidean distance threshold of 3.0. Using compacity as shape attribute allows to efficiently discriminate moles from other bright structures of the saturation image (see Figure 3, right, for comparison).

Acknowledgements

References

[1]   E. J. Breen and R. Jones, *Attribute openings, thinnings, and granulometries*, Computer Vision and Image Understanding **64** (1996), no. 3, 377–389.

[2]   L. Chen, M. W. Berry, and W. W. Hargrove, *Using dendronal signatures for feature extraction and retrieval*, International Journal of Imaging Systems and Technology **11** (2000), no. 4, 243–253.

[3] P. Dokládal, I. Bloch, M. Couprie, D. Ruijters, R. Urtasun, and L. Garnero, *Topologically controlled segmentation of 3D magnetic resonance images of the head by using morphological operators*, Pattern Recognition **36** (2003), no. 10, 2463–2478.

[4] S. Fischer, P. Schmid, and J. Guillod, *Analysis of skin lesions with pigmented networks*, Proceedings of the International Conference on Image Processing (ICIP'96), 1996, pp. 323–326.

[5] M. Grimaud, *New measure of contrast: dynamics*, Image Algebra and Morphological Image Processing III, July 1992, pp. 292–305.

[6] P. Hanusse and P. Guillataud, *Sémantique des images par analyse dendronique*, RFIA'91 - Reconnaissance des Formes et Intelligence Artificielle, 1991, pp. 577–588.

[7] R. Jones, *Connected filtering and segmentation using component trees*, Computer Vision and Image Understanding **75** (1999), no. 3, 215–228.

[8] J. Mattes and J. Demongeot, *Efficient algorithms to implement the confinement tree*, DGCI'00 - Discrete Geometry for Computer Imagery, 2000, pp. 392–405.

[9] B. Naegel and N. Boch, *Un système d'aide au diagnostic dermatologique par cartographie et suivi de grains de beauté*, Proceedings of the french conference orasis 2007, 2007.

[10] L. Najman and M. Couprie, *Building the component tree in quasi-linear time*, IEEE Transactions on Image Processing **15** (2006), no. 11, 3531–3539.

[11] G. K. Ouzounis and M. H. F. Wilkinson, *Second-order connected attribute filters using max-trees*, ISMM'05 - International Symposium on Mathematical Morphology, 2005, pp. 65–74.

[12] _____ , *Mask-based second-generation connectivity and attribute filters*, IEEE Transactions on Pattern Analysis and Machine Intelligence **29** (2007), no. 6, 990–1004.

[13] P. Salembier, A. Oliveras, and L. Garrido, *Anti-extensive connected operators for image and sequence processing*, IEEE Transactions on Image Processing **7** (1998), no. 4, 555–570.

[14] P. Schmid-Saugeon, J. Guillod, and J. P. Thiran, *Towards a computer-aided diagnosis system for pigmented skin lesions*, Computerized Medical Imaging and Graphics **27** (2003), 65–78.

[15] J. Serra, *Image Analysis and Mathematical Morphology. Vol 2. Theoretical Advances*, Academic Press, London, 1988.

[16] E. R. Urbach, *Vector attribute filters*, ISMM'05 - International Symposium on Mathematical Morphology, 2005, pp. 95–104.

[17] _____ , *Connected shape-size pattern spectra for rotation and scale-invariant classification of gray-scale images*, IEEE Transactions on Pattern Analysis and Machine Intelligence **29** (2007), no. 2, 272–285.

[18] E. R. Urbach and M. H. F. Wilkinson, *Shape-only granulometries and gray-scale shape filters*, ISMM'02 - International Symposium on Mathematical Morphology, 2002, pp. 305–314.

[19] C. Vachier, *Utilisation d'un critère volumique pour le filtrage d'image*, RFIA'98 - Reconnaissance des Formes et Intelligence Artificielle, 1998, pp. 307–315.

[20] L. Vincent, *Morphological area openings and closings for grey-scale images*, NATO Shape in Picture Workshop, 1992, pp. 197–208.

[21] _____ , *Grayscale area openings and closings, their efficient implementations and applications*, EURASIP Workshop on Mathematical Morphology and its Applications to Signal Processing, 1993, pp. 22–27.

[22] D. Zhang and G. Lu, *Review of shape representation and description techniques*, Pattern Recognition **37** (2004), no. 1, 1–19.